13th IEA Heat Pump Conference
April 26-29, 2021 Jeju, Korea

A Dynamic Model for Microchannel Heat Exchanger under Frost Conditions

Jiazhen Ling[a,*], Lingzhe Wang[b], Rohit Dhumane[c], Vikrant Aute[a]

[a]Center for Environmental Energy Engineering, Univresity of Maryland, College Park, Maryland, 20742, USA
[b]Center for Sustainability in the Built Environment, University of Maryland, College Park, Maryland, 20740, USA
[c]Modine Manufacturing Company, 1500 Dekoven Ave, Racine, Wisconsin, 53403, USA

Abstract

Heat pump manufacturers gradually adopt microchannel heat exchangers (MCHX) as the outdoor coils due to the compactness and lower cost. The relatively small hydraulic diameter of MCHX also enhances the heat transfer compared to traditional tube and fin coils. However, such benefits may turn to a challenge when heat pumps operate under the frost condition. Air flow is easily blocked when frost builds up in the smaller flow channels formed by the fins and microchannel tubes. To study the MCHX performance under frost condition, we developed a Modelica-based dynamic model that accounts for the performance degradation under frost conditions. The MCHX is modeled using the finite volume method and the sensible and latent heat transfer between refrigerant and moist air is solved using both heat and mass conservation equations. Regarding the frost accumulation, the model considers both the frost densification and thickness growth which will reduce the conductivity of the tube surface and the minimum free flow area, leading to poor air-side heat transfer. The model can also be applied on a heat pump system along with other in-house developed Modelica component models to assist the understanding of heat pump COP degradation during frost.

Selection and/or peer-review under responsibility of the organizers of the 13th IEA Heat Pump Conference 2020.

Keywords: Heat pump; microchannel heat exchangers; frost simulation; transient/dynamic modeling

1. Introduction

In winter, heat pump systems are typically more energy efficient in providing heating than electric heaters or gas fired furnaces. Following the principle of the Carnot Cycle, heat pumps can transform the low-grade ambient heat to higher-grade space heat, making the cycle Coefficient of Performance (COP) higher than one. The popularity of heat pumps in many places of the world has been motivating researchers and engineers to further improve the system efficiency and reduce the cost. To that end, microchannel heat exchangers (MCHX) gain momentum in heat pump installations. MCHX, being widely used in the automotive AC industry, has a typical hydraulic diameter of 1 mm which is much smaller than the ones of tube-and-fin heat exchangers (TFHX). The small hydraulic diameter leads to compactness since the increase of heat transfer area-to-volume ratio is accompanied by the decrease of hydraulic diameter. Khan and Fartaj [1] conducted a literature review on MCHX in which the MCHX's compactness was corroborated by the example that a state-of-the-art multi-port flat tube heat exchanger registered a capacity per volume in the range of 2-3 MW/m^3. Although, it goes without saying that using MCHX in heat pumps is advantageous, there are still challenges faced by the traditional TFHXs, that MCHXs cannot address better. One such challenge is the frost-induced performance degradation during winter operations. As the outdoor unit becomes evaporator during a heat pump operation, its surface temperature may be lower than both the freezing point and the dewpoint of ambient air. Frost can therefore accumulate on the evaporator and as a result, the thermal resistance of the evaporator increases, eventually deteriorating the heat pump efficiency.

* Corresponding author. Tel: 1-301-405-8270
Email: jiazhen@umd.edu

To mitigate the frost built-up and its negative impact on cycle performance, we need to understand how frost first appears and distributes on the evaporator; how the increased thermal resistance due to frost built-up alters the operation of vapor compression cycle; lastly how the altered VCC operation reciprocates on the frost accumulation. Those questions can be answered either through experimental or numerical studies. Henry Barrow [2] was among the first to register his concern over frost accumulation in heat pumps. Through his fin model, he concluded the increased thermal resistance due to frost were majorly caused by air flow blockage, and the impact from lower thermal conductivity of frost was secondary. Moallem et al. [3] experimentally measured both the frost thickness and weight accumulated over two evaporators used in air source heat pumps. They used a digital scale to measure the frost weight and a CCD camera to capture the frost thickness growth over time. They concluded the frost onset was highly dependent on local fin temperature and the frost grew faster when the water vapor content of incoming air is higher. The same group of researchers [4] later developed a semi-empirical model that predicts non-uniform frost growth on heat exchangers. The model adopts a quasi-steady state, heat and mass balance-based segment-by-segment approach.

This paper introduces a Modelica-based full dynamic microchannel heat exchanger model with frost prediction capability, as opposed to a quasi-steady state approach, and further applies the model on a vapor compression cycle model, so that the impact from frost accumulation on cycle operation can be quantified. As suggested in the above literature, a comprehensive frost model should consider both the frost densification process which impacts the fin surface thermal conductivity and the frost thickness growth which blocks air passage through the heat exchanger. By exercising the model, we would like to demonstrate that it is a helpful tool when conducting research on: how frost first appears and distributes on the evaporator? How the increased thermal resistance due to frost built-up alters the operation of vapor compression cycle?

2. Modeling Methodology

The modeling methodology includes two main pieces: a segment-by-segment based microchannel model and a frost model that serves as an add-on to the first one. The microchannel model further includes three control volumes: the air-side control volume, the refrigerant-side control volume and the fin and flat-tube wall control volume. The frost model is applied to air-side control volume only so that the frost simulation will not be constrained to particular geometries of the MCHX as well as the refrigerant flowing inside the MCHX flat tube.

2.1 Segment-by-segment based microchannel heat exchanger model

The above-mentioned control volumes are better visualized in Figure 1. In the direction of flat tubes, the heat exchanger is divided into a number of segments which comprise the three control volumes. The structure of the control volumes enables the reusability of each control volume for other types of heat exchangers. The green ports and red ports are Fluidports and Heatports, respectively. They both act as connectors and by connecting those ports to each other, a set of conservation equations are established (Eq. 1 – 4). Eqn. 2 and 3 also carry the information of flow direction through the positive and negative signs.

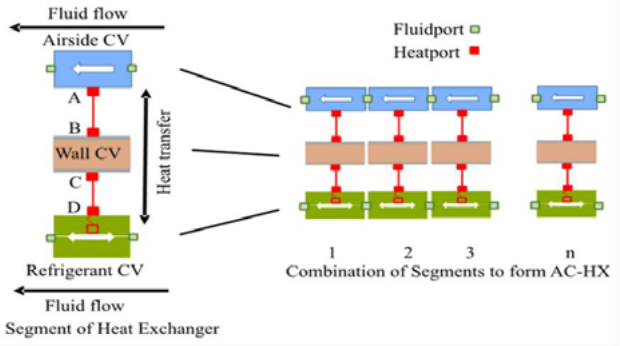

Figure 1 Subcomponent structure for MCHX model

Fluidports: $P_1 = P_2$ (1)

$$\dot{m}_1 + \dot{m}_2 = 0 \quad (2)$$

$$\dot{m}_1 h_1 + \dot{m}_2 h_2 = 0 \quad (3)$$

Heatports: $\dot{q}_1 + \dot{q}_2 = 0$ (4)

The refrigerant-side control volume is a lumped model which merges the multiple MCHX ports into a single tube (see Figure). The implicit assumptions here are that the refrigerant maldistribution among the ports are neglected and consequently there is a single temperature along the width of the tube (width here means length along the airflow direction). According to Li et al. [5], such an assumption tends to neglect the refrigerant maldistribution in each port which could lead to a heat exchanger level capacity degradation of 3.6%.

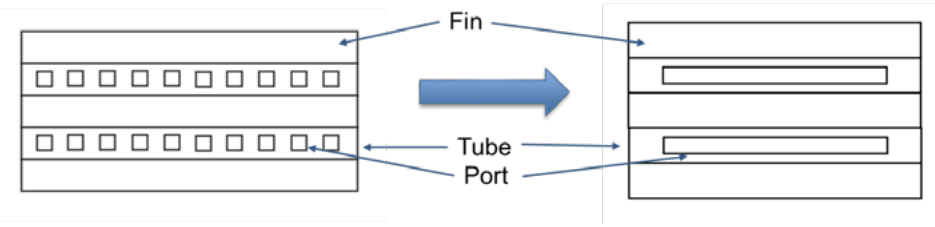

Figure 2: Refrigerant-side port-level simplification for MCHX model

The tube temperature for the lumped port profile of the model MCHX is evaluated as discussed below. The thickness δ_t is evaluated from Equation 5, using the tube height (H_t) and port height (H_p). The tube mass (m_t) is obtained from Equation 6, where n_t is number of tubes and ρ_t is the tube material density. The fin mass (m_f) of MCHX is evaluated from Eqn. 7, where A_s is surface area, t_f is fin thickness and ρ_f is fin material density. Weighted averages of specific heat capacity (c) and mass (m) from Equations 8 and 9 are used in the energy equation for the tube control volume to evaluate the dynamic temperature profile in Equation 10. Q_a and Q_r are heat flows to air-side and refrigerant-side respectively.

$$\delta_t = \frac{H_t - H_p}{2} \quad (5)$$

$$m_t = n_t \rho_t L_t (H_t W_t - A_c) \quad (6)$$

$$m_f = \frac{A_s}{2} t_f \rho_f \quad (7)$$

$$c = \frac{m_t c_t + m_f c_f}{m_t + m_f} \quad (8)$$

$$m = m_t + m_f \quad (9)$$

$$mc \frac{dT}{dt} = \dot{Q}_a + Q_r \quad (10)$$

The Q_a term is evaluated in the airside control volume. Fin efficiency η is used to combine primary and secondary heat transfer areas into a single effective heat transfer area (Eqn. 11). The primary and secondary areas for heat transfer are evaluated from Eqns. 12 and 13. The number of fins per unit length (called fin density) is represented by ξ. Pt is the tube pitch (distance between consecutive tubes).

$$A_e = A_p + \eta A_f \quad (11)$$

$$A_p = 2L_t(W_t + H_t - \xi t_f W_t) \quad (12)$$

$$A_s = 2L_t \xi \left[W_t (P_t - H_t) + P_t (W_f - W_t) \right] \quad (13)$$

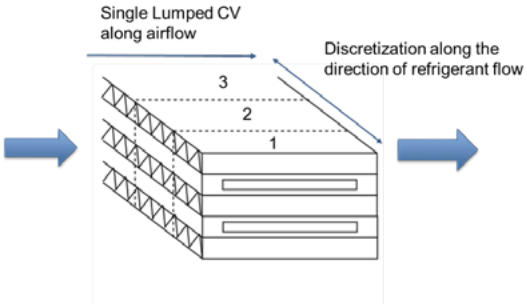

Figure 3: Discretization of airside control volume

The heat transfer coefficient for airside is critical for accurate evaluation for heat transfers. A linear correlation developed from experimental data is fed into the model for improved accuracy. The face area (A_f) is evaluated from geometrical parameters by Eqn. 14.

$$A_f = (n_t - 1)P_t + L_t \tag{14}$$

$$u = \frac{\dot{V}}{A_f} \tag{15}$$

$$\alpha = min\left(\left(\frac{\tilde{\alpha}}{\tilde{u}}\right)u, \alpha_0\right) \tag{16}$$

Face velocity (u) is obtained from volume flow rate ($\dot{V}$) using Eqn. 15 and is used as independent parameter for heat transfer coefficient (α) evaluation from the empirical Eqn. 16, obtained from manufacturing data. To model natural convection at zero flow rate, a condition happens during cycle shut down or mode switch, a minimal volume flow rate can be provided to get non-zero heat transfer coefficient values for zero flow case. The correlating terms $\tilde{\alpha}$and $\tilde{u}$are obtained from the linear trend line passing through origin. Epsilon-NTU method is used to evaluate air outlet temperature and airside heat transfer capacity (Q_a) can be now evaluated using the values of total heat transfer area, heat transfer coefficient and air temperatures.

The refrigerant-side control volume contains dynamic mass and energy conservation equations. Pressure and enthalpy are the state variables used for evaluating other thermo-physical quantities and for the progress in time. Homogenous model of void fraction is used in the model for faster simulation time because the refrigerant charge distribution is not critical parameter for evaluation.

2.2 Frost model

As discussed earlier, a complete frost model should consider both the frost thickness and the frost densification. Figure 4 describes the modeling approach that captures basic frost phenomenon [6].

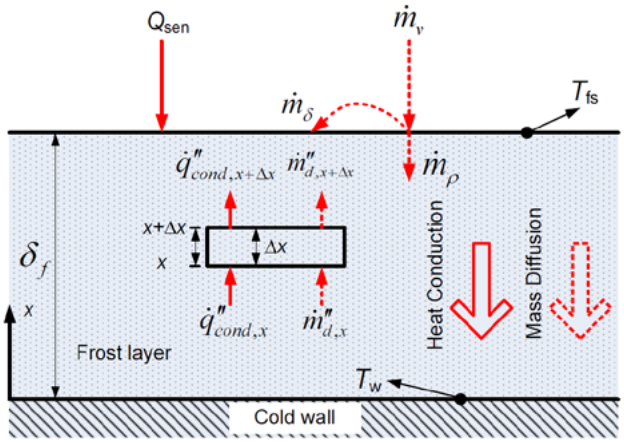

Figure 4: Schematic for frost modeling [6]

In Figure 4, the MCHX fin surface is generalized as a cold surface and the dotted shades represent the frost layer. The x direction points to the frost growth direction. As cold and moist air flows on the top of the cold surface at T_w, moisture deposits on the surface at a rate of $\dot{m}_v$, and turns to frost. The air stream rejects both sensible heat, Q_{sen}, and latent heat, in the condensate rate of $\dot{m}_v$, to the MCHX surface covered by frost. The condensate, $\dot{m}_v$, may either deposit on top of the fresh frost or, through the gap of topmost frost, deposit in the middle of the frost layer, resulting both the frost thickness growth, in the rate of $\dot{m}_\delta$, and the frost densification, in the rate of $\dot{m}_\rho$, respectively. As a result, the frost thickness, δ_f, and the frost density increases, the latter of which further affects the frost layer thermal conductivity. The basic frost accumulation phenomenon embodies a heat and mass transfer process, so the governing equations applied to the control volume are shown in Eqns. 17 and 18.

Mass Balance:

$$\dot{m}''_{d,x} - \dot{m}''_{d,x+\Delta x} = -\frac{\partial \dot{m}''_{d,x}}{\partial x}\Delta x = \frac{\partial}{\partial t}(\rho_f \Delta x) \tag{17}$$

Energy Balance:

$$\Delta x\left[-\frac{\partial q''_{cond,x}}{\partial x} - \frac{\partial}{\partial x}\left(\dot{m}''_d h_v\right)\right] = \frac{\partial}{\partial t}(\rho_f h_f \Delta x) \tag{18}$$

For the sake of simplicity, the paper omits the detailed mathematical deduction which can be found in [6] and only presents the solutions to the above governing equations. In addition, an empirical equation is used to connect the frost densification to the change of frost thermal conductivity.

Water vapor absorbed by the frost layer:

$$\dot{m}''_\rho = \frac{\zeta p_{v,sat}(T_w)}{R_v T_w \varphi}\sinh(\varphi \delta_f) \tag{19}$$

Where

$$\zeta = D_{eff}\{\frac{1}{\delta_f}cosh^{-1}[\frac{T_w}{T_{fs}}\frac{p_{v,sat}(T_{fs})}{p_{v,sat}(T_w)}]\}^2 \tag{20}$$

$$\varphi = \sqrt{\frac{\zeta}{D_{eff}}} \tag{21}$$

The average density of frost for the next time step:

$$\bar{\rho}_{f,t+\Delta t} = \bar{\rho}_{f,t} + \frac{\dot{m}_{\rho}^{"}}{\delta_f}\Delta t \tag{22}$$

The frost thickness for the next time step:

$$\delta_{f,t+\Delta t} = \delta_{f,t} + \frac{\dot{m}_{v}^{"} - \dot{m}_{\rho}^{"}}{\bar{\rho}_{f,t}}\Delta t \tag{23}$$

The thermal conductivity of the frost layer [7]:

$$k_f = 0.132 + 3.13 \times 10^{-4}\bar{\rho}_f + 1.6 \times 10^{-6}{\bar{\rho}_f}^2 (50 < \bar{\rho}_f < 400 \frac{kg}{m^3}) \tag{24}$$

3. Case study: Frost accumulation prediction on MCHX in a heat pump

With the help of the model described above, we can now analyze the frost accumulation by reviewing the air-side control volume of each segment. In the scope of this paper, the focus is to explore the frost thickness growth, the increase of frost density as well as the related frost thermal conductivity change on different locations of a MCHX. Furthermore, we want to compare the heat pump frost performance over two MCHX pass configurations: one pass and two-pass.

3.1 Heat pump system

The details of the system, a 3-ton R410A heat pump using a scroll compressor and thermal expansion valve (TXV), are described in [8] with only one replacement to the outdoor unit. A microchannel HX replaced the original tube-and-fin heat exchanger. Table 1 shows the dimensions of the microchannel heat exchanger.

Table 1: The one pass MCHX parameters

Refrigerant pass configuration	1 pass
Total number of flat tubes	48
Tube length (mm)	50
Tube pitch (mm)	2.54
Number of ports in a tube	10
Port height/width (mm/mm)	1/1
Fin type	Flat fin
Fins per inch	12

The operating condition of the heat pump follows the frost accumulation condition pursuant to ASHRAE Standard 116 (1995) [9]: the outdoor air condition is 1.7°C/0.7°C (dry bulb/wet bulb) and the indoor air condition is 21.1°C/13.2°C (dry bulb/wet bulb).

3.2 Prediction of frost growth, densification of MCHX

Since dynamic simulations require initial values to determine the solutions for the future time steps, the surface temperature, as shown in Figure 5, of MCHX is assumed to be 3K warmer than the incoming air at time 0. As vapor compression cycle starts, the refrigerant flowing inside the evaporator gradually cools the fin surface and in about 80 seconds, the fin surface temperature drops below the freezing point. It has to be noted that the system uses TXV to regulate the outlet superheat and thus, there will be an initial time region in which refrigerant temperature fluctuates, responding to the superheat adjustment by the TXV. This fluctuation is reflected on the surface temperature profile which rises and drops shortly after reaching sub-freezing temperature region. The surface temperature eventually stabilizes, and the last two segments are in superheated region. It needs to be noted that we only showed four out of ten segments' results for all plots in this section. This is because all simulation results show Segments 1 through 6, and Segments 7 and 8 have very similar predicted values. So, to clearly show the results and avoid putting a line on top of each other, we only reported the four segments that can best represent the trend of frost distribution. Figure 6 shows the frost growth in each MCHX segment. Segment 1 is the section closest to the inlet and Segment 10 is the section closest to the outlet, and the other segments fall in places in between. The frost starts to grow at about 80 seconds which coincides with the time at which surface temperature of the heat exchanger falls below the freezing point. The frost growth rate is very close to linear and its slope is determined by the frost surface temperature, and it is intuitive that the superheat region of the heat exchanger has the least amount of frost covered.

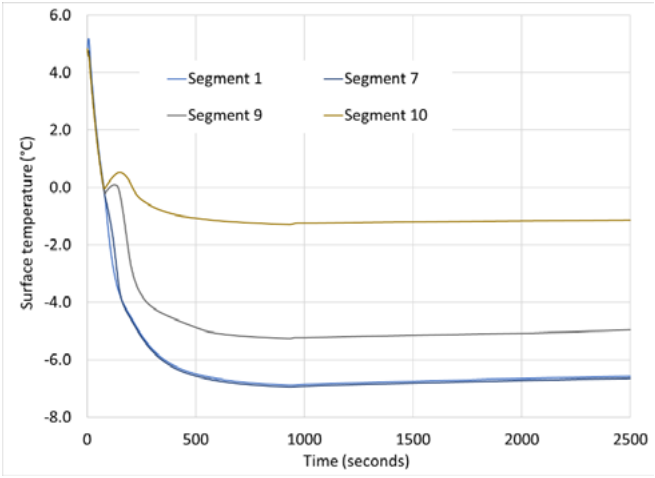

Figure 5: The surface temperature distribution over MCHX

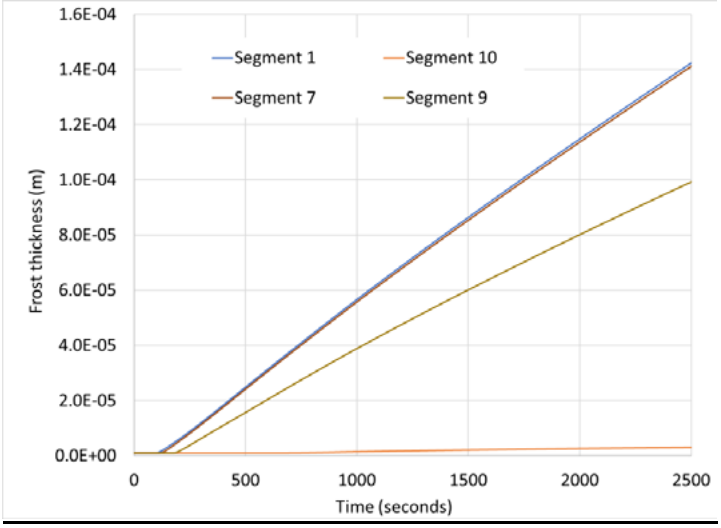

Figure 6: The frost thickness distribution over MCHX

Regarding the second aspect of frost accumulation, we use Figure 7 to examine the frost density distribution over the MCHX. To avoid any singularities, the initial frost density is assumed to be 30 kg/m^3 or 0.03 g/cm^3 [6,10]. Unlike the frost thickness growth, the frost densification process is non-linear and those segments closer to the evaporator outlet have slightly denser frost which are caused by the significantly smaller frost thickness. As shown in Figure 7, the densification of frost increases the frost thermal conductivity but such a level of increase is shadowed by the growth of frost thickness and, as as a result, the change of overall thermal resistance is dominant by the frost thickness growth.

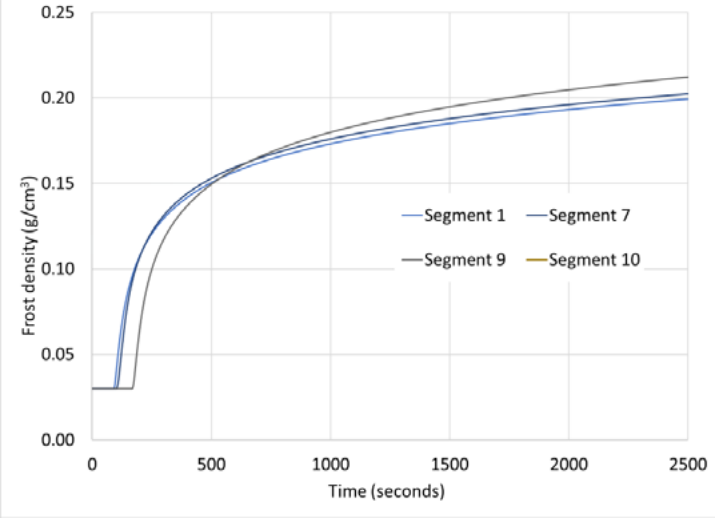

Figure 7: The frost density distribution over MCHX

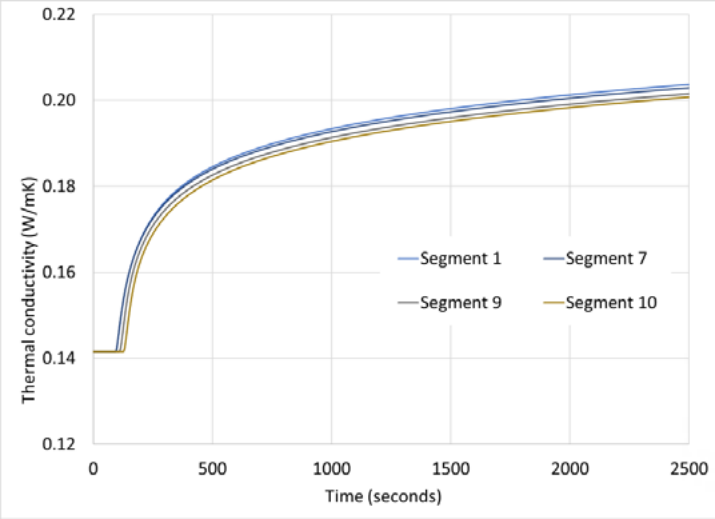

Figure 8: The frost thermal conductivity distribution over MCHX

To summarize, the increase in frost thickness will increase the thermal resistance between air and the refrigerant. The change in thermal conductivity due to frost densification plays a minor role in the change of thermal resistance. This can be observed by the fact that the change of thermal conductivity in Figure 8 is on relatively a smaller scale compared to the frost thickness growth. The net impact from both, the increase of frost thickness and frost density, is the increase of thermal resistance that impedes the heat transfer of air to refrigerant in the outdoor unit. The reduction of thermal conductive resistance is not the only reason for the cycle performance deterioration under frost conditions. As pointed out by Henry Barrow, there is yet another important factor contributing to the heat pump frost operation: air flow blockage. As frost grows among tubes and fins, the effective air flow passage becomes smaller, increasing the air-side pressure drop. Figure 8 depicts such a phenomenon. The air-side pressure drop doubles the amount than the non-frost value when assuming the air flow through the evaporator maintains constant. This also doubles the power of the fan in order to overcome the flow resistance. It has to be pointed out that in reality, the fan power usually remains constant and as a result, the air flow rate will decrease due to the increase of air side pressure drop. This further impairs the cycle capacity and COP. In the future, the current model will be improved by considering the air flow reduction during frost accumulation.

3.3 MCHX flow pass configuration to heat pump operation under frost condition

MCHXs are typically one or more passes as shown in Figure 9 [11]. By using a buffer (separator), refrigerant is restricted to flow into part of the tubes comprising the first pass, as opposed to flow into all tubes in the case of one pass. The refrigerant then turns 180° and flows into the rest of tubes comprised of the second pass. For an evaporator, the two-pass design expands the refrigerant as it turns into vapor, causing higher mass flux in tubes which may lead to better heat transfer and potentially higher pressure drop. However, since the air-side heat transfer remains dominant and such dominance is further amplified in the frost condition, the benefits of using two-pass over one-pass in heat transfer could be further depreciated. To make a closer examination, we established a two-pass MCHX that maintains all specifications of the one-pass design with the only modification that the flat tubes are divided into two passes: 8 tubes in the first pass and 40 tubes in the second pass.

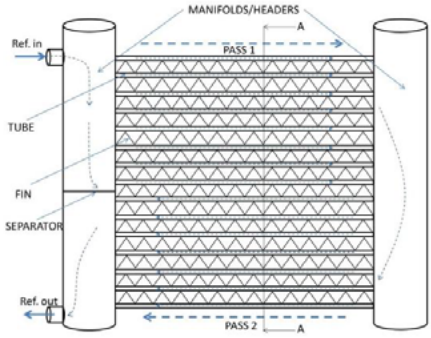

Figure 9: A sample view of Mircochannel Heat Exchanger

Figure 10 compares the pressure levels of the same heat pump system using one pass MCHX and two-pass MCHX. The two systems show almost identical pressure levels and only to compare the second digit after the decimal, one concluded that one-pass MCHX leads to both higher evaporating and condensing pressure levels. If we further compare the heat pump COP, which is demonstrated in Figure 11, we notice the COP is also similar and we have to compare the third digit after the decimal to conclude the two-pass MCHX leads a slightly larger heat pump performance. Such a close result is anticipated because the air-side condition is identical to the two evaporators and frost intensifies the air-side heat resistance dominance, meanwhile reduces the impact of better refrigerant-side heat transfer. In fact, at time when frost is yet to accumulate (t <80 seconds), we can notice the two pass MCHX cycle has a clearer edge in COP which disappears as frost builds up.

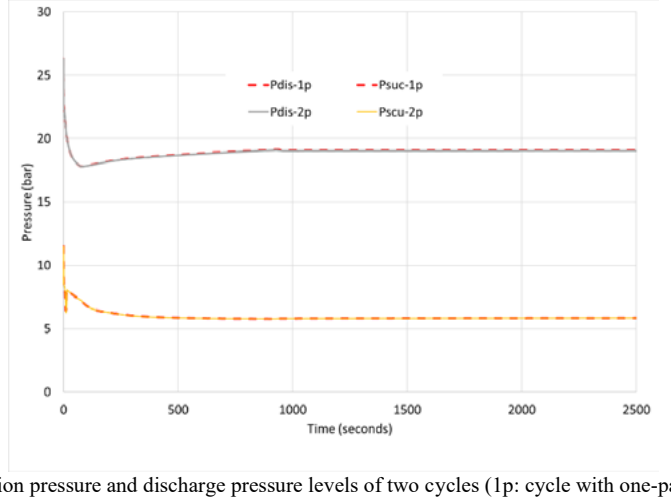

Figure 10: Suction pressure and discharge pressure levels of two cycles (1p: cycle with one-pass MCHX; 2p: cycle with two-pass MCHX)

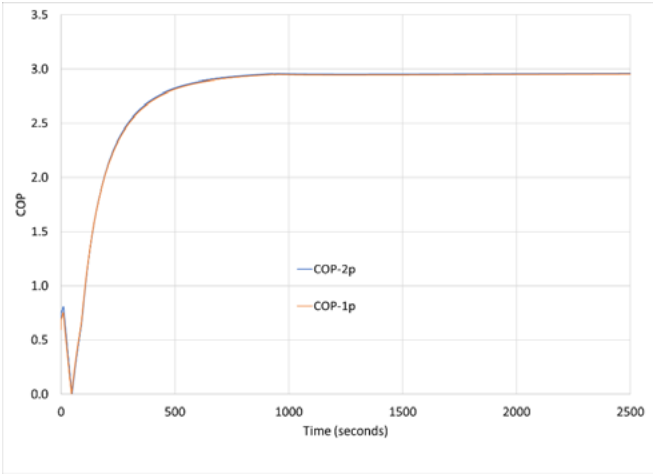

Figure 11: Coefficient of Performance (COP) of two cycles (1p: cycle with one-pass MCHX; 2p: cycle with two-pass MCHX)

4. Conclusions

The paper presents a numerical study on the operation of heat pump system with microchannel heat exchanger during frost accumulation. We modeled the microchannel heat exchanger using a segment-by-segment approach and lumped the multiple ports in the flat tube into one flow channel. The frost model is applied to the air-side control volume of the heat exchanger model so that it can be extended to other types of heat exchanger. We modeled the basic frost phenomena including frost densification and thickness growth. Through a set of case studies, we determined the frost growth on a heat exchanger depended mostly on the heat exchanger surface temperature. Regarding the heat transfer resistance due to frost accumulation, the thermal conductivity change due to the frost densification is apparently a secondary factor shadowed by the frost thickness growth. On a cycle-level comparison, we did not find significant performance enhancement by using a two-pass microchannel heat exchanger. We believe the dominance of air-side heat transfer resistance is further intensified by frost accumulation and as a result, the COP improvement from the two-pass MCHX is very much limited.

Acknowledgements

This work was supported by the Modeling and Optimization Consortium (MOC) at the University of Maryland.

References

[1] Khan M. G. and Fartaj A., 2011, A review on microchannel heat exchangers and potential applications.
[2] *Int. J. Energy Res.*, 35: 553–582
[3] Barrow H., 1985, A note on frosting of heat pump evaporator surfaces, *J. of Heat Recovery sys.*,
[4] 5 (3), 1985, 195-201
[5] Moallem E., Padhmanabhan S., Cremaschi L., Fisher D.E., 2010, Experimental study of onset and growth of rost on outdoor coils of air-srouce heat pump systems, *ASME-ATI-UIT 2010 Conference on Thermal and Environmental Issues in Energy Systems, 16-19 May, 2010, Sorrento, Italy*
[6] Padhmanabhan S., Fisher D.E., Cremaschi L., Moallem E., Modeling non-uniform frost growth on a fin-and-tube heat exchanger, *Int. J. of Ref.,* 34 (8), 2011, 2018-2030

[7] Li Z., Ling J., Aute V., Radermacher R., 2017, Investigation of Port Level refrigerant flow maldistribution in microchannel heat exchanger, 12th IEA Heat Pump Conference, Rotterdam, Netherland
[8] Qiao H., 2014, Transient modeling of two-stage and Variable Refrigerant Flow Vapor Compression Sytems with Frosting and Defrosting, PhD dissertation, University of Maryland, College Park
[9] Lee, J., Byun J.S., 2009, Experiment on the performance improvement of air-to-air heat pump adopting the hot gas bypss method by outdoor fan speed, Journal of Mechanical Science and Technology 23, 2009, 3407-3415
[10] Alabdulkarem Abdullah, Yunho Hwang, Reinhard Radermacher, 2013, System Drop-In Tests of Refrigerants R-32, D2Y-60, and L-41a in Air Source Heat Pump, *Air-Conditioning, Heating, and Refrigeration Institute Low-GWP Alternative Refrigerants Evaluation Program, Test report #20*, University of Maryland, College Park
[11] ASHRAE Standard 116 (1995) Methods of Testing for Rating Seasonal Efficiency of Unitary Air Conditioners and Heat Pumps
[12] Le Gall R., Grillot J.M., Jallut C., 1997, Modeling of frost growth and densification, International Journal of Heat Mass Transfer, Vol. 40, No. 13, pp. 3177-3187
[13] Mehendale S., Aute V., Radermacher R., Principles of refrigerant circuit optimization in single row microchannel condensers, 2014 Purdue Conference-Compressor short course, July 13, 2014